# Membrane Charge and Curvature Determine Interaction with Acyl-CoA Binding Protein (ACBP) and Fatty Acyl-CoA Targeting†

Hsu Chao,‡ Gregory G. Martin,§ William K. Russell,|| Suryakant D. Waghela,‡ David H. Russell,|| Friedhelm Schroeder,§ and Ann B. Kier*,‡

*Departments of Pathobiology, Physiology and Pharmacology, and Chemistry, Texas A&M University, TVMC, College Station, Texas 77843-4467*

*Received April 11, 2002; Revised Manuscript Received June 17, 2002*

ABSTRACT: Although acyl-CoA binding protein (ACBP) stimulates utilization of long-chain fatty acyl-CoA by a variety of membrane-bound enzymes, it is not known whether ACBP directly interacts with membranes. To test this hypothesis, mouse recombinant (mr) ACBP was engineered to contain the native mouse ACBP amino acid sequence expressed as a fusion protein at high levels (>150 mg/L) in *Escherichia coli*. Purification and cleavage of the fusion tag resulted in mrACBP identical to native ACBP as shown by mass (10000.5 Da) and amino acid sequence (peptide mapping after proteolysis) determined by matrix-assisted laser desorption time of flight (MALDI-TOF) mass spectroscopy. The mrACBP was functionally active as shown by binding of *cis*-parinaroyl-CoA with high affinity, $K_d = 12 \pm 2$ nM, at a single binding site, stimulating oleoyl-CoA utilization by microsomal glycerol-3-phosphate acyltransferase 3.2-fold and protecting oleoyl-CoA from microsomal acyl-CoA hydrolase. Direct interaction of mrACBP with membranes was demonstrated by two independent methods: (i) Circular dichroism showed an 8% increase in α-helix content of mrACBP in the presence of anionic phospholipid-rich, but not neutral, small unilamellar vesicles (SUV). (ii) Membrane filtration confirmed that mrACBP bound to anionic phospholipid-rich SUV but only weakly interacted with neutral SUV or large unilamellar vesicles (LUV), regardless of charge. (iii) The mrACBP−oleoyl-CoA complex transferred 2−3-fold more oleoyl-CoA to anionic phospholipid-rich SUV than to anionic phospholipid-rich LUV and neutral SUV or LUV. Conversely, mrACBP extracted less oleoyl-CoA from anionic phospholipid-rich SUV. Taken together, these data indicated for the first time that mrACBP interacted preferentially with anionic phospholipid-rich, highly curved membranes to facilitate transfer of ACBP-bound ligands.

Long-chain fatty acyl-CoAs (LCFA-CoAs) are important intermediates in fatty acid metabolism and also have important physiological functions in regulating gene transcription, signal transduction (protein kinase C), ion channels, ion pumps, enzymes of lipid metabolism (e.g., acetyl-CoA carboxylase, HMG-CoA reductase), and membrane trafficking (*1*−*3*). Because of these effects of LCFA-CoAs, it is important for mammalian cells to regulate the level and/or intracellular targeting of LCFA-CoAs to maintain normal physiological functions. Although several intracellular proteins have been discovered that bind LCFA-CoAs (*1*), only acyl-CoA binding protein exclusively binds $C_{12}$−$C_{22}$ LCFA-CoAs with high affinity ($K_d = 2$−10 nM) (*1*). Acyl-CoA binding protein (ACBP)[1] is primarily a 10 kDa cytosolic protein, highly conserved and widely distributed among all eukaryotic organisms and tissues tested (*1*, *4*).

The three-dimensional structure of bovine apo-ACBP and holo-ACBP (palmitoyl-CoA bound) was recently elucidated by nuclear magnetic resonance (NMR) spectroscopy (*5*) and differential polarized phase fluorometry (*6*). ACBP consists of 86−103 amino acids, which fold into four α-helix bundles covering the sequence from amino acids 2−11, 20−38, 51−62, and 72−85 (*5*). The α-helices form a shallow bowl-like structure that forms the binding pocket for long-chain fatty acyl-CoAs (LCFA-CoAs). Upon ligand binding, ACBP undergoes significant conformational change as evidenced by 23% decreased rotational correlation time, by 2 Å decrease in overall hydrodynamic diameter, and increased segmental motions of ACBP tryptophan (Trp) residues (*6*). $^{15}N$ relaxation NMR measurements confirmed that the ACBP backbone dynamics are influenced by ligand binding (*7*). Taken together, these alterations indicate that ACBP undergoes conformational changes upon binding of LCFA-CoAs.

Because the ligand binding site of ACBP is highly specific for LCFA-CoAs and does not bind fatty acids or lipids that form membrane bilayers (cholesterol and phospholipids) (*1*), the possibility that ACBP may bind to membranes has not previously been considered. Nevertheless, in vitro studies suggest that ACBP mediates a variety of reactions involving

† This work was supported in part by the USPHS, National Institutes of Health Grant DK41402.

* To whom correspondence should be addressed. Phone: (979) 862-1509. Fax: (979) 845-9231. E-mail: Akier@cvm.tamu.edu.

‡ Department of Pathobiology, Texas A&M University.

§ Department of Physiology and Pharmacology, Texas A&M University.

|| Department of Chemistry, Texas A&M University.

[1] Abbreviations: ACBP, acyl-CoA binding protein; mrACBP, mouse recombinant ACBP with amino acid sequence identical to mouse native ACBP; L-FABP, liver fatty acid binding protein; SCP-2, sterol carrier protein-2; BSA, bovine serum albumin; SUV, small unilamellar vesicle; LUV, large unilamellar vesicle; CD, circular dichroism.

10.1021/bi0259498 CCC: $22.00 
Published on Web 07/20/2002

and/or occurring in membranes including intermembrane LCFA-CoA transport (*8*), extracting/donating LCFA-CoAs from/to membranes (*8*), binding LCFA-CoAs and protection from microsomal hydrolysis (*9*), donating LCFA-CoAs to mitochondria to enhance LCFA-CoA $\beta$-oxidation (*8*), removing LCFA-CoAs from mitochondrial fatty acyl-CoA synthetase (end product-inhibited enzyme) (*10*), donating LCFA-CoAs to microsomal glycerol-3-phosphate acyltransferase and acylglycerol-3-phosphate acyltransferase to stimulate phosphatidic acid synthesis (*9*), and inducing membrane fusion (*1*−*3*).

Despite these data suggesting that ACBP interacts with membranes to elicit its effects, direct ACBP−membrane interaction has heretofore not been reported. Precedent for such a possibility, however, is based on the fact that other intracellular LCFA-CoA binding proteins such as sterol carrier protein-2 (SCP-2) (*11*) and liver fatty acid binding protein (L-FABP) (*12*) preferentially bind to anionic phospholipid-rich, highly curved membranes. Just like ACBP, SCP-2 (*13*) and L-FABP have high affinity for LCFA-CoA (*14*, *15*), stimulate microsomal glycerol-3-phosphate acyltransferase to enhance phosphatidic acid synthesis (*9*, *16*), and protect LCFA-CoA from microsomal hydrolases (*9*, *17*). On the basis of the similarity of these activities, it is postulated that ACBP may also preferentially interact with anionic phospholipid-rich, highly curved membranes.

The purpose of the present investigation was to determine if (i) ACBP interacts with membranes, (ii) ACBP exhibits a preference for binding anionic phospholipid-rich, highly curved membranes, and (iii) ACBP preferentially donates/extracts LCFA-CoA to/from phospholipid-rich, highly curved membranes. While native ACBP can be prepared from mouse liver, the presence of high levels of L-FABP complicates the isolation as evidenced by the fact that ACBP was first isolated as an impurity of L-FABP prepared from liver (*18*). Since earlier studies showed that small differences in amino acid sequence in the N-terminus of ACBP could significantly alter function (*19*) while alterations in the N-terminal α-helical region of SCP-2 prevented interaction with membranes (*11*), a purified mouse recombinant acyl-CoA binding protein (mrACBP) with amino acid sequence identical to that of the native mouse ACBP was prepared (*20*).

## MATERIALS AND METHODS

*Materials.* Recombinant bacteria producing mrACBP were constructed with commercially available molecular biological reagents. The pET32/Xa/LIC vector, NovaBlue and BL21-(DE3) host cells, S-protein−agarose, factor Xa, and Xarrest agarose were purchased from Novagen (Madison, WI). Primers were synthesized by Integrated DNA Technologies (Coralville, IA). Ni-NTA agarose, Qiaprep spin mini-prep kit, and Qiaquick PCR purification kit were purchased from Qiagen (Valencia, CA). AmpliTaq Gold PCR kit and restriction enzymes were purchased from Roche (Indianapolis, IN). Protein was determined by Bradford assay using a kit purchased from Bio-Rad (Hercules, CA).

B-PER bacterial protein extraction reagent was purchased from Pierce (Rockford, IL), and Complete Mini protease inhibitor cocktail tablets were purchased from Roche (Indianapolis, IN). Sephacryl S-300 beads were acquired from Amersham (Uppsala, Sweden). Stirred cells (models 8400 and 8050), cellulose acetate membrane (YM, cutoff 10 and 3 kDa), Microcon YM-3 and YM-100 centrifugal filter devices, and Immobilon-P and Immobilon-CD (PVDF) membranes were purchased from Fisher Scientific (Pittsburgh, PA). Protein molecular weight markers were purchased from Bio-Rad or Amersham (Uppsala, Sweden). For SDS−PAGE gels the protein bands were visualized with Coomassie Blue or Gelcode Blue stains from Pierce Chemical Co. (Rockford, IL).

Cholesterol (3$\beta$-hydroxy-5-cholesten-3-one), triacylglycerol, cholesteryl oleate, 1-palmitoyl-2-oleoyl-*sn*-glycero-3-phosphocholine (POPC), and 1,2-dioleoyl-*sn*-glycero-3-phospho-L-serine (DOPS) were purchased from Avanti Polar Lipids (Alabaster, AL). [1-$^{14}$C]Oleoyl-CoA (56.3 mCi/mmol) was obtained from Perkin-Elmer (Boston, MA). Silica gel 60 thin-layer chromatography plates were obtained from EM Science (Gibbstown, NJ). All other chemicals were of reagent grade or better.

*Construction of a mrACBP/pET32Xa/LIC Plasmid with His and S-Tags.* The mouse ACBP EST clone (Gene Bank Accession No. W98643) was purchased from Genome System (Palo Alto, CA) and its coding sequence confirmed. Plasmid DNA was prepared by Qiagen spin mini-prep kit and sequenced by the GENE Technology Laboratory (Department of Biology, Texas A&M University, College Station, TX). The DNA sequencing reactions were done by PCR amplification using the T3 or T7 primers.

The mrACBP cDNA coding sequence was then amplified by polymerase chain reaction (PCR) using the forward primer (5′-GTATTGAGGGTCGC*ATG*TCTCAGGCTGAATTTG-3′) and the reverse primer (5′- AGAGGAGAGTTAGAGC-CCTGGTGAT*TTA*TATTCCGT-3′) containing ligation-independent cloning (LIC) site compatible sequences (underlined) and the ATG initiation and the TTA stop codon (italicized), respectively. PCR was performed with AmpliGold Taq polymerase under denaturing conditions at 94 °C, 10 min, 30 cycles of 94 °C for 30 s, 60 °C for 30 s, and 72 °C for 30 s, with a final 7 min extension at 72 °C. The PCR product was purified using QiaQuick PCR purification kit and quantitated on a 1% agarose gel. The purified PCR fragment was treated with T4 DNA polymerase to generate the LIC-compatible cohesive ends and then ligated into the pET32/Xa/LIC plasmid vector by incubating the insert and vector at room temperature for 5 min. The ligation mixture was used to transform NovaBlue bacteria (Novagen, Madison, WI). NovaBlue is end$^-$ and rec$^-$ for higher transformation efficiency and plasmid yield. Positive clones with mrACBP plasmid (mACBP/pET32/Xa) were selected by colony PCR, and the presence of insert was confirmed by restriction enzyme analysis. Positive plasmid sequences were further confirmed by DNA sequencing. For expression of high levels of the His and S-tag mrACBP fusion protein, the His and S-tag mrACBP/pET32/Xa plasmid was transformed into BL21(DE3) bacteria.

*Expression of mrACBP Fusion Protein in Escherichia coli.* For large-scale His and S-tag mrACBP fusion protein expression, a starter culture of 8 mL of $LB_{amp}$ broth (containing 100 $\mu$g of ampicillin/mL) was inoculated with a single bacterial colony which was incubated at 37 °C for 8 h. The bacteria were pelleted, the supernatant was removed, the pellet was resuspended in 3 mL fresh $LB_{amp}$ broth, and 1.5 mL of this bacterial suspension was added to 500 mL of

$LB_{amp}$ broth. The large culture was incubated at 37 °C with shaking (225 rpm) until the $OD_{600}$ reached 0.5−1.0. Isopropyl $\beta$-thiogalactopyranoside (IPTG) was added to the culture to a final concentration of 1 mM, and the incubation was continued for another 2 h. The bacteria were pelleted by centrifugation at 6000*g* for 10 min. The bacterial pellet was drained and resuspended in 60 mL of B-PER reagent (Pierce, Rockford, IL) supplemented with one Complete protease inhibitor tablet (Roche, Indianapolis, IN) and incubated at room temperature for 15 min with gentle shaking to allow for thorough lysis of the bacteria. The homogenate was centrifuged at 27200*g* for 15 min. The supernatant containing the soluble protein was collected and frozen at −70 °C. Sodium dodecyl sulfate−polyacrylamide gel electrophoresis (SDS−PAGE) and Western blots were done to assess the expression of mrACBP fusion protein.

*Purification of mrACBP Fusion Protein.* The mrACBP fusion protein was purified by affinity chromatography using S-tag agarose. The affinity chromatography was performed in a batchwise method. Ten milliliters of soluble protein solution was incubated with 30 mL of S-tag agarose in a 125 mL Econo-Column (Bio-Rad) at room temperature for 1 h with gentle shaking. The shaking allowed thorough binding to the agarose. At the end of 1 h, the flow-through was collected. The S-tag agarose was resuspended in a full column volume of S-tag bind/wash buffer (20 mM Tris-HCl, pH 7.5, 150 mM NaCl, 0.1% Triton X-100) and briefly incubated at room temperature with gentle shaking. The procedure was repeated a total of five times. The S-tag agarose was washed further by running 2 L of bind/wash buffer through the column. The bound protein was eluted by adding 60 mL of $MgCl_2$ and incubating at room temperature for 10 min. The column was eluted once more, and the eluate was pooled.

*Factor Xa Cleavage.* To cleave both fusion tags from mrACBP fusion protein, the S-tag bind/wash buffer was exchanged with factor Xa cleavage buffer (50 mM Tris-HCl, pH 8.0, 100 mM NaCl, 5 mM $CaCl_2$) using ultrafiltration with a Microcon Model 8200 stirred cell (Fisher Scientific, Pittsburgh, PA). The protein was concentrated with the stirred cell until the protein concentration was 2.5−3 mg/mL. Protein quantitation was done using the Bio-Rad protein assay kit. The S-tag agarose purified mrACBP fusion protein was cleaved with factor Xa at a ratio of 15 $\mu$g of protein/unit of factor Xa. The cleavage mixture was incubated at 37 °C overnight. At intervals, aliquots of the protein cleavage mixture were separated using tricine SDS−PAGE and stained with Coomassie Blue to confirm protein cleavage. Factor Xa was removed by incubating the cleavage solution with Xarrest agarose in a 50 mL Econo-Column for 10 min at room temperature. The cleavage mixture (containing mrACBP, some uncleaved mrACBP fusion protein, and cleaved fusion tags) was then allowed to flow through the column.

*Final Purification of mrACBP with Native Peptide Sequence.* To further remove uncleaved mrACBP fusion protein and residual fusion tags, the buffer was first changed to S-tag bind/wash buffer by ultrafiltration as above. Purification of mrACBP with the native peptide sequence was accomplished by incubating the cleavage protein mixture (in S-tag bind/wash buffer) with S-tag agarose at room temperature for 1 h to remove the uncleaved mrACBP fusion protein and bound nonspecific protein. The flow-through was collected, and the buffer was changed to Ni-NTA binding buffer by ultrafiltration. The protein solution was then incubated with Ni-NTA agarose at 4 °C overnight with gentle shaking. The flow-through containing the mrACBP was transferred to a dialysis bag (cutoff 3000 Da) and dialyzed at least six times against no less than 150 volumes of 50 mM Tris-HCl, pH 7.4, buffer at 4 °C with stirring. The protein was concentrated by ultrafiltration with the stirred cell. Purified mrACBP was quantitated using the Bio-Rad protein assay kit.

*Tricine Sodium Dodecyl Sulfate−Polyacrylamide Gel Electrophoresis.* Protein samples were prepared for electrophoresis by the addition of an equal volume of buffer containing glycerol, 2-mercaptoethanol, 100 mM Tris-HCl, SDS, and Coomassie G-250. Samples were electrophoresed in 16.5% tricine gels as described by Schagger and von Jagow (*21*). Gels not used for immunoblotting were stained with Coomassie stain (0.1% Brilliant Blue R-250) or Gelcode Blue stain to detect the protein.

*Western Blotting.* Rabbit antiserum to native ACBP derived from mouse LM cell fibroblasts, prepared as described previously (*19*), showed no cross-reaction with fatty acyl-CoA binding proteins (liver, heart, and intestine) or the sterol carrier protein-2 (*19*). For immunoblotting of proteins resolved by SDS−PAGE, the proteins were transferred to PVDF membranes at 30 V overnight using a Miniprotean II transblot apparatus (Bio-Rad, Hercules, CA). The membranes were allowed to air-dry briefly at room temperature and were then blocked in a solution of 5% nonfat dry milk/Tris-buffered saline/0.05% Tween 20 (TBST) for 2 h. Membranes were then incubated with primary antibody (i.e., rabbit anti-LM cell ACBP) in TBST/1% BSA at a 1:1000 dilution for 2 h and washed 2 × 15 min with TBST and 1 × 15 min with TBS. Membranes were then incubated with secondary antibody (horseradish peroxidase-conjugated goat anti-rabbit IgG) obtained from Sigma Chemical Co. (St. Louis, MO) at a 1:4000 dilution in TBST for 1 h. Finally, the blots were washed three times for 15 min with Tris-buffered saline (TBS). Visualization of ACBP was accomplished using the chromagen (4-chloro-1-naphthol) in the presence of 0.1% hydrogen peroxide.

*Mass Spectrometry.* Mass spectra of mrACBP and proteolytic peptides were obtained by matrix-assisted laser desorption ionization linear time of flight (MALDI-linear TOF) Voyager Elite XL TOF mass spectrometer (PerSeptive Biosystems, Framingham, MA) equipped with delayed extraction (*19*, *22*). Each sample was prepared using the overlayer method of sample preparation (*22*). Briefly, 1 mL of a 0.15 M α-cyano-4-hydroxycinnamic acid solution in methanol was applied to the stainless steel sample plate and allowed to dry. A solution of the matrix and the purified mrACBP was then prepared in 2:1 water:methanol with final matrix and protein concentrations of 10 and 4 $\mu$M, respectively. Then 0.5 mL of this solution was applied over dried matrix crystals. Salts were removed by washing the sample spots with a drop of ultrapure water and shaking off the excess after 10 s. Each spectrum represents the average of 100 laser shots. The spectrum of each mrACBP preparation was acquired in the delayed-extraction linear mode, with a total acceleration of 25 kV, a pulse voltage of 2 kV, and a delay time of 200 ns. These mass spectra were externally calibrated using a calibration curve generated from a sample spot containing ubiquitin ($M_r$ 8565) and cytochrome *c* ($M_r$

12360.1). The $[M + H]^+$ ion values reported consist of the mass of the protein plus the addition of a proton (hydrogen ion) due to ionization of the protein by the MALDI-TOF technique. $M_r$ represents the mass of the protein without the proton.

*Protein Digestion and Mass Spectrometric Peptide Sequencing.* Small molecules were removed from purified mrACBP using an NID Removal MicroTrap cartridge in combination with a desalting trap (Michrom Bioresources, Inc., Auburn, CA). The resulting mrACBP was then divided into three aliquots and enzymatically digested using trypsin, chymotrypsin, or Glu-C (all sequence grade; Roche, Indianapolis, IN) as previously described (*19*, *22*). All conditions were identical except for a 12 h analysis period and maintaining the chymotrypsin solution at room temperature. Two microliter aliquots of each solution were sampled and mixed with 2 $\mu$L of matrix solution (0.1 M $\alpha$-cyano-4-hydroxycinnamic acid, 0.2% formic acid, methanol). The resulting mixture was spotted onto a gold-plated target plate that had previously been coated with a thin layer of $\alpha$-cyano-4-hydroxycinnamic acid. The masses were obtained using a Voyager Elite XL TOF mass spectrometer (PerSeptive Biosystems, Framingham, MA) using the delayed-extraction reflectron mode and the following instrument settings: acceleration voltage 25 keV, 70% grid voltage, 0.008% guide wire voltage, and a delay of 150 $\mu$s.

The mrACBP was also analyzed using an in-gel digest. The gel electrophoresis was performed using a Bio-Rad Mini Protean 3 (Bio-Rad Laboratories, Hercules, CA) and a 14% T polyacrylamide gel. The in-gel digest procedure was similar to that of Rosenfeld et al. (*23*).

*N-Terminal Amino Acid Sequencing.* The factor Xa cleavage mixture and the final purified mrACBP native protein were separated by tricine SDS−PAGE and transferred to PVDF membranes. The membranes were stained with Coomassie Blue and amino acid sequenced by the Protein Chemistry Laboratory at the University of Texas Medical Branch (Galveston, TX). The mrACBP was sequenced for 15 cycles revealing the N-terminal 15 amino acids.

*Fluorescent cis-Parinaroyl-CoA Binding Assay. cis*-Parinaroyl-CoA is a naturally occurring, 18-carbon, fluorescent LCFA-CoA whose structure resembles that of oleoyl-CoA (*6*). *cis*-Parinaroyl-CoA binding characteristics of mrACBP were determined as described previously for rat native ACBP (*6*), human recombinant SCP-2 (*13*), and rat native L-FABP (*15*).

*Effect of mrACBP on Rat Liver Microsomal Phosphatidic Acid Biosynthesis.* The microsomal biosynthesis of phosphatidic acid from glycerol 3-phosphate (G3P) was determined under conditions optimized previously for recombinant L-FABP (*9*). Gel-washed microsomes were prepared as described previously (*9*, *16*, *24*, *25*). Briefly, each 50 $\mu$L reaction mixture contained 15 mM dithiothreitol, 70 mM Tris-HCl (pH 7.4), 735 $\mu$M G3P, 80 mM NaF, 40 $\mu$M [1-$^{14}$C]-oleoyl-CoA, and mrACBP or doubly distilled $H_2O$ as a control. The reaction mixture was preincubated for 15 min at 37 °C in a water bath. The reaction was initiated by addition of 10 $\mu$g of the microsomal protein, and the reaction was permitted to proceed for 15 min at 37 °C in a water bath. The lipids were then extracted and separated by thin-layer chromatography (*9*, *16*, *24*, *25*) using silica gel 60 plates in a solvent system containing chloroform/methanol/acetic acid/doubly distilled water (50:37.5:3.5:2 v/v). Bands corresponding to phosphatidic acid were scraped and counted for $^{14}$C using a liquid scintillation counter (Packard 1600TR, Meridan, CT). Each reaction was carried out in at least triplicate. Values represent the mean ± SEM.

*Effect of mrACBP on Rat Liver Microsomal Hydrolysis of Oleoyl-CoA.* Microsomal hydrolase activity for [1-$^{14}$C]-oleoyl-CoA was determined as described previously (*9*, *17*).

*Preparation of Small (SUV) and Large (LUV) Unilamellar Vesicles.* Membrane vesicles were comprised of 1-palmitoyl-2-oleoylphosphatidylcholine (POPC) and cholesterol with or without dioleoylphosphatidylserine (DOPS). SUV composed of POPC/cholesterol (molar ratio 65:35) or POPC/cholesterol/DOPS (55:35:10) were prepared essentially as described previously (*11*, *20*, *26*), with some modifications. Lipids dissolved in chloroform stocks were mixed in an amber vial, dried under $N_2$ to form a thin film on the wall of the vial, and rehydrated in 10 mM Tris-HCl buffer, pH 7.4, prefiltered through a 0.2 $\mu$m filter (Millipore, Bedford, MA).

SUV were prepared by subjecting the rehydrated the lipid mixture to vigorous vortexing and sonication for 5 min in a water bath sonicator at room temperature. Then the lipid mixture was sonicated on ice under $N_2$ with a sonicator (Sonic Dismembrator Model 550, Fisher Scientific, Pittsburgh, PA). The lipid mixture was sonicated for 15 cycles, each cycle consisting of 2 min sonication followed by 1 min pause with a set power output level of 4. Multilamellar and large vesicles and debris from the sonicator probe were removed by centrifugation at 110000*g* for 4 h at 4 °C using a 40Ti rotor (Beckman Instruments, Fullerton, CA). To make the LUV, the lipid suspension was extruded using a hand-held mini-extruder (Avanti, Alabaster, AL). The extrusion was repeated 15 times between double layers of 0.1 $\mu$m polycarbonate membranes (Avanti, Alabaster, AL). A lipid phosphate assay was used to determine the lipid concentration of the final SUV solution.

*Binding of mrACBP to Liposomal Membranes: Circular Dichroism.* Circular dichroic spectra of samples containing buffer only or mrACBP protein (2.5 $\mu$M) with or without lipid vesicles (1.25 mM) were measured as described (*11*). Samples containing buffer only and samples containing liposome without mrACBP were used as control for background subtraction. A J-710 spectropolarimeter (JASCO, Easton, MD) was used to obtain the CD measurements. All measurements were made at room temperature for samples in a 1 mm circular quartz cell. The spectra were obtained across the range of 185−260 nm under the following conditions: 1 nm step resolution; 50 nm/min; response 1 s; bandwidth 2.0 nm; sensitivity 0.01°. Each measurement was the average of 10 scans, which was smoothed, background-subtracted, and converted to mean residue molar ellipticity ($deg \cdot cm^2 \cdot dmol^{-1}$). The percentage $\alpha$-helix for the mrACBP protein was estimated by using the SELCON program.

*Binding of mrACBP to Liposomal Membranes: Trp and Tyr Steady-State Fluorescence Emission Spectroscopy.* Steady-state fluorescence spectra of mrACBP Trp and Tyr were obtained in a 1 cm quartz cuvette utilizing a PC1 photon counting spectrofluorometer (ISS Instruments, Champaign, IL). Buffer only (10 mM potassium phosphate, pH 7.4) or buffer containing 500 $\mu$M SUV without mrACBP was used as a control for background subtraction. The sample temperature was maintained at 25 ± 0.1 °C. Each sample was

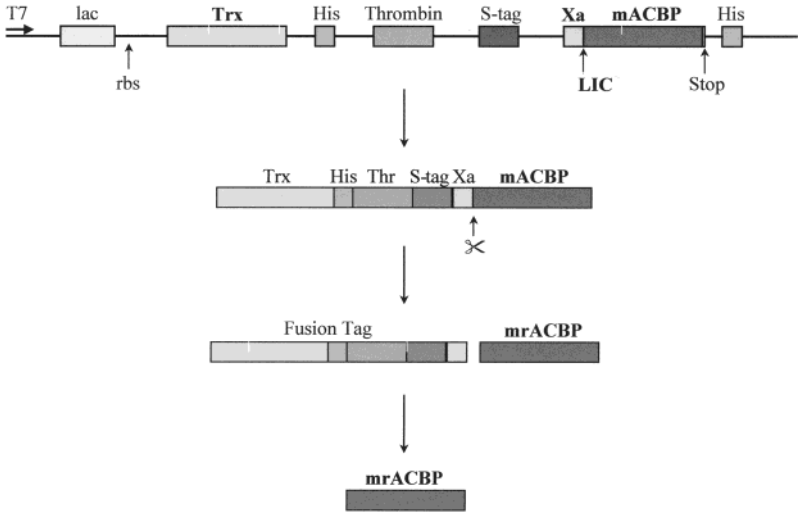


FIGURE 1: Mouse recombinant ACBP/pET32Xa/LIC plasmid construct and native mrACBP purification scheme. The mouse ACBP cDNA coding sequence containing the stop codon was inserted into the LIC cloning site as described in Materials and Methods. The *E. coli* expressed fusion peptide containing the thioredoxin, thrombin, histidine, and S-tag peptide sequences and a factor Xa protease cleavage site was cleaved with factor Xa to release the native mrACBP. Fusion peptide and factor Xa were removed as described in Materials and Methods to yield mrACBP.

allowed to equilibrate for 2−3 min in the spectrofluorometer prior to data collection. Excitation and emission bandwidths were 4 and 8 nm, respectively. The mrACBP was excited at 270 nm (excites both Trp and Tyr) or at 296 nm (selectively excites Trp).

*Binding of mrACBP to Liposomal Membranes: Nucleopore Filtration.* The binding of mrACBP to SUV and LUV was performed as described previously (*20*). mrACBP (2.5 $\mu$M) and 1.25 mM vesicles in 300 $\mu$L of 10 mM Tris-HCl, pH 7.4, buffer were incubated at room temperature for 15 min. The mixture was then centrifuged in a Microcon-100 filtration unit (cutoff 100000 Da) at 3000*g* in a benchtop centrifuge until all solution passed through the membrane. The flow-through fraction was lyophilized and rehydrated in 100 $\mu$L of doubly distilled water. Six microliters of the protein solution was separated on 16.5% tricine gel and stained with Coomassie Blue for protein quantitation. An internal standard curve composed of 0.1, 0.2, 0.5, and 0.8 $\mu$g of the mrACBP was run on each gel. The protein quantitation was performed using the Scion Image software (Scion Corp., Frederick, MD).

*Binding of Oleoyl-CoA to Liposomal Membrane.* [1-$^{14}$C]-Oleoyl-CoA (2 $\mu$M) was incubated with 750 $\mu$M liposomes for 10 min at room temperature in 100 $\mu$L of 10 mM Tris-HCl, pH 7.4, buffer for measuring the binding of [1-$^{14}$C]-oleoyl-CoA to liposome. At the end of the incubation, the sample was centrifuged at 10000*g* in a YM-3 filter apparatus until the filtration membrane was dry. The flow-through was transferred to a scintivial and counted in a liquid scintillation counter. An identical sample without liposome was used as a control to ensure that the [1-$^{14}$C]oleoyl-CoA passed through the YM-3 filter. Liposomes (SUV or LUV) did not pass through the YM-3 filter (*11*, *20*, *26*).

*Transfer of mrACBP-Bound Oleoyl-CoA to the Liposomal Membrane.* The mrACBP/oleoyl-CoA complex was formed by mixing 2.5 $\mu$M mrACBP and 2 $\mu$M [1-$^{14}$C]oleoyl-CoA in 100 $\mu$L of 10 mM Tris-HCl, pH 7.4, buffer and incubating the mixture at room temperature for 10 min. To ensure that the [1-$^{14}$C]oleoyl-CoA and mrACBP/[1-$^{14}$C]oleoyl-CoA complex both passed through the YM-3 filter, each was added separately and as a complex to the filtration cartridge and centrifuged at 10000*g* at room temperature until the surface of the membrane was dry. The filtrate and retentate were counted as described above. To measure transfer of [1-$^{14}$C]-oleoyl-CoA from a preformed mrACBP/[1-$^{14}$C]oleoyl-CoA complex to liposome, the mrACBP/[1-$^{14}$C]oleoyl-CoA complex (2.5 $\mu$M:2 $\mu$M) was incubated with 750 $\mu$M liposome at room temperature for 10 min in 100 $\mu$L of 10 mM Tris-HCl, pH 7.4, buffer. The sample was then centrifuged at 10000*g* in a YM-100 filter column. The filtrate and the retentate were counted as previously mentioned. The same sample without the liposomes was used as control.

*Extraction of Liposome-Bound Oleoyl-CoA by mrACBP.* To measure extraction of membrane-bound [1-$^{14}$C]oleoyl-CoA by mrACBP, the mrACBP was incubated with the liposome/[1-$^{14}$C]oleoyl-CoA complex in 100 $\mu$L of 10 mM Tris-HCl, pH 7.4, buffer at room temperature for 15 min. The mixture was then centrifuged at 10000*g* in a YM-100 filter apparatus until the membrane surface was dry, and again the filtrate and retentate were measured in a liquid scintillation counter.

## RESULTS

*Cloning, Expression, and Purification of Recombinant Mouse ACBP.* Since small amino acid sequence differences in the N-terminal portion of ACBP significantly alter its structure (*27*) and function (*19*), it was essential to prepare mrACBP identical to the native mouse ACBP. This was accomplished by constructing an expression plasmid using the mouse ACBP EST clone with a coding sequence identical to that of the mouse DBI gene (*28*) and PCR engineered to insert the mouse ACBP cDNA coding region into the pET32/Xa/LIC vector (Figure 1). The mouse recombinant mrACBP cDNA encoded the entire 87 amino acids including the initial methionine into the pET32/Xa/LIV vector using the LIC site. The stop codon was inserted at the 3′ end to avoid the 5′ end fusion peptide. Insertion of the cDNA into the LIC site allowed cleavage of the 5′ end fusion peptide and purification of the mrACBP. The pET32/Xa/LIC vector had several 5′

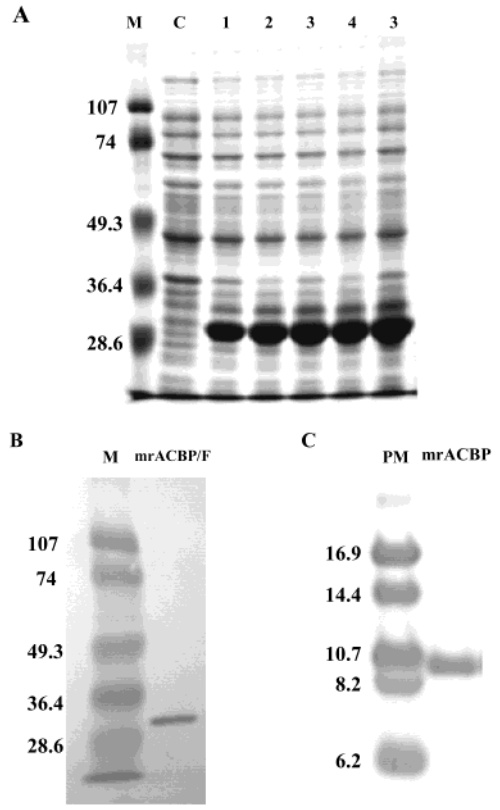


FIGURE 2: Expression of mouse recombinant ACBP (mrACBP) in BL21(DE3) *E. coli*. Panel A: Five mrACBP/pET32XA/LIC clones (1−5) expressed mrACBP fusion protein of about 28 kDa. The control clone C did not have a dense 28 kDa protein band that showed on the gel. Panel B: S-protein−agarose purified mrACBP fusion protein showed a single band on the Coomassie Blue stained gel. Panel C: The final purified native mrACBP (C) showed a single 10 kDa band on the Gelcode Blue stained gel. Symbols represent the following: M, Bio-Rad prestained SDS−PAGE low-range molecular standards; C, the control bacteria clone C without the mrACBP/pET32Xa/LIC plasmid; mrACBP/F, the mrACBP fusion protein; PM, Amersham peptide marker; mrACBP, final purified mrACBP.

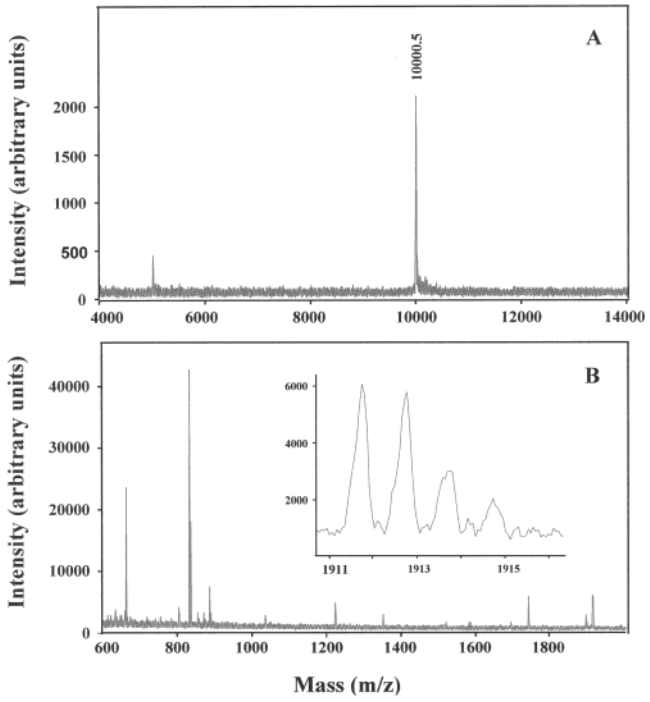


FIGURE 3: Linear delayed-extraction MALDI-TOF mass spectral analysis of the mrACBP sequence. Panel A: MALDI-TOF of mrACBP. Panel B: the tryptic digested fragment of native mrACBP. The observed $M_r$ was 10000.5. The insets containing the *m*/*z* showed that the resolution is sufficient to resolve the carbon isotopes.

end tags: the thioredoxin tag, which increased the solubility of the fusion protein; the S-tag and the His-tag, both of which were used for affinity purification; the thrombin and factor Xa sites, which allowed the proteolytic cleavage of the fusion protein using thrombinase or factor Xa.

Driven by the T7 promoter, the mrACBP fusion protein near 28 kDa was highly expressed in BL21 cells (Figure 2A) as shown by SDS−PAGE gels and achieved levels >150 mg/L. Almost all the mrACBP fusion protein was soluble, consistent with the presence of the thioredoxin tag which increased solubility. Only trace amounts of mrACBP appeared in bacterial inclusion bodies. Purification of mrACBP fusion protein was achieved by sequential affinity chromatography, i.e., S-protein−agarose purification followed by Ni-NTA agarose purification to yield a single band on Coomassie Blue stained SDS−PAGE gels (Figure 2B). The mrACBP fusion protein was completely cleaved by factor Xa (15 $\mu$g of fusion protein/unit of factor X) to yield 10 kDa mrACBP, the complete 18 kDa fusion peptide, as well as 14 kDa and 2 kDa fragments resulting from partial digestion of the 18 kDa fusion peptide (confirmed by peptide sequencing; data not shown). The 18 and 14 kDa peptides were removed using S-tag agarose and Ni-NTA agarose affinity chromatography. The smallest band was removed by membrane dialysis. The final purified mrACBP from which all tags had been removed appeared as a single band on Gelcode Blue stained SDS−PAGE gels (Figure 2C). Equivalent immunoreactivity of equal amounts of protein on western blotting (not shown) indicated that the mrACBP shared domains similar to those of the mouse native ACBP. Based on >150 mg of mrACBP fusion protein/L in the bacteria, the overall yield of mrACBP was 42%, approximately 62 mg/L of pure mrACBP.

*Determination of mrACBP Mass.* To determine if the mass of mrACBP was identical to that of mouse native ACBP, MALDI-TOF-MS analysis was performed using a Voyager Elite XL TOF mass spectrometer in linear mode. An intense signal, corresponding to the $[M + H]^+$ ion of mrACBP, was observed at 10000.5 Da (Figure 3A). The $[M + H]^+$ and the $[M + 2H]^{2+}$ ions of cytochrome *c* were used as internal standards. On the basis of the cDNA-derived amino acid sequence of mrACBP (identical to native mouse ACBP), the calculated mass of the $[M + H]^+$ ion of mrACBP should have been 10000.6 Da. With an instrumental accuracy of 0.1 Da/10000.0 Da, the measured and predicted molecular weights were the same.

*N-Terminal Amino Acid and Peptide Sequencing of mrACBP.* The first 15 amino acids of purified mrACBP were identical to mouse native ACBP (Figure 4). To determine if the rest of the mrACBP sequence was also identical, mrACBP was proteolytically digested by trypsin (Figure 3B) and other enzymes as described in Materials and Methods, followed by analysis of the resulting fragments by MALDI-TOF to determine the molecular mass of each fragment. The proteolytically digested mrACBP fragment masses covered the entire sequence of mrACBP (Table 1), verifying that the

```
1   MSQAEFDKAA  EEVKRLKTQP  TDEEMLFIYS  30
    **************************************
31  HFKQATVGDV  NTDRPGLLDL  KGKAKWDSWN  60

61  KLKGTSKESA  MKTYVEKVDE  LKKKYGI     87
            ********************************
```

FIGURE 4: Amino acid sequence of mrACBP. The first 15 amino acids were sequenced. Symbols represent the observed tryptic fragment (—), observed chymotrypsin fragment (···), observed Glu-C fragment (∗), and observed in-gel tryptic fragment (bold).

Table 1: Mass Assignment of Proteolytic Fragments of mrACBP

| fragment sequence | *m/z* | | |
|---|---|---|---|
| | measured | calculated | Δ |
| $Met^{1}-Lys^{14}$ | 1582.698 | 1582.742 | −0.044 |
| $Met^{1}-Arg^{15}$ | 1738.830 | 1738.843 | −0.013 |
| $Ala^{9}-Lys^{15}$ | 802.452 | 802.442 | 0.010 |
| $Leu^{16}-Lys^{33}$ | 2227.124 | 2227.110 | 0.014 |
| $Gln^{34}-Lys^{51}$ | 1912.013 | 1912.013 | −0.000 |
| $Ala^{54}-Lys^{61}$ | 1034.480 | 1034.505 | −0.025 |
| $Thr^{73}-Lys^{82}$ | 1223.651 | 1223.652 | −0.001 |
| $Thr^{73}-Lys^{83}$ | 1351.760 | 1351.747 | −0.013 |
| $Asp^{49}-Tyr^{56}$ | 945.533 | 945.552 | −0.021 |
| $Asn^{60}-Met^{71}$ | 1293.690 | 1293.683 | 0.007 |
| $Lys^{63}-Tyr^{74}$ | 1330.640 | 1330.667 | −0.027 |
| $Val^{75}-Ile^{87}$ | 1548.880 | 1548.900 | −0.020 |

mrACBP peptide sequence was identical to that of the mouse native ACBP.

*Structure of mrACBP*. Although the above data demonstrated that the primary amino acid sequence and mass of mrACBP were identical to those of the mouse native ACBP, it was necessary to determine if mrACBP adopted a structure similar to that of the mouse native ACBP. Therefore, the secondary structure of mrACBP was measured by circular dichroism. Circular dichroic spectra of mrACBP in an aqueous buffer showed a negative ellipticity of −15700 deg·cm$^2$·dmol$^{-1}$ at 222 nm and large positive ellipticity of 36430 deg·cm$^2$·dmol$^{-1}$ at 190 nm (Figure 5A, solid circles). These findings suggested a large α-helix content. Analysis of the CD spectrum as indicated in Materials and Methods showed that mrACBP had 56% α-helix, consistent with NMR data of native ACBP (*4*, *5*).

*Functional Activity of mrACBP: LCFA-CoA Binding.* To determine if the mrACBP was functionally active, its ability to bind *cis*-parinaroyl-CoA (a naturally occurring fluorescent LCFA-CoA) was examined in a fluorescence binding assay not requiring separation of bound from free ligand as described in Materials and Methods. The assay was based on the fact that *cis*-parinaroyl-CoA fluoresces weakly in aqueous solution, but this fluorescence signal increases dramatically upon interaction with proteins containing hydrophobic ligand binding sites (*13*, *15*). In the presence of mrACBP, the fluorescence intensity of *cis*-parinaroyl-CoA increased with increasing ligand concentration in a saturable manner (Figure 6). A Scatchard plot of the binding data was linear, indicating a single binding site (Figure 6, inset). Analysis of the Scatchard plots from three experiments showed that mrACBP bound *cis*-parinaroyl-CoA with a $K_d$ = 12 ± 2 nM at a single binding site, $n$ = 0.95 ± 0.13 mol/mol. These ligand binding characteristics were very similar to those reported previously for mouse native ACBP and rat native ACBP (*6*, *19*).

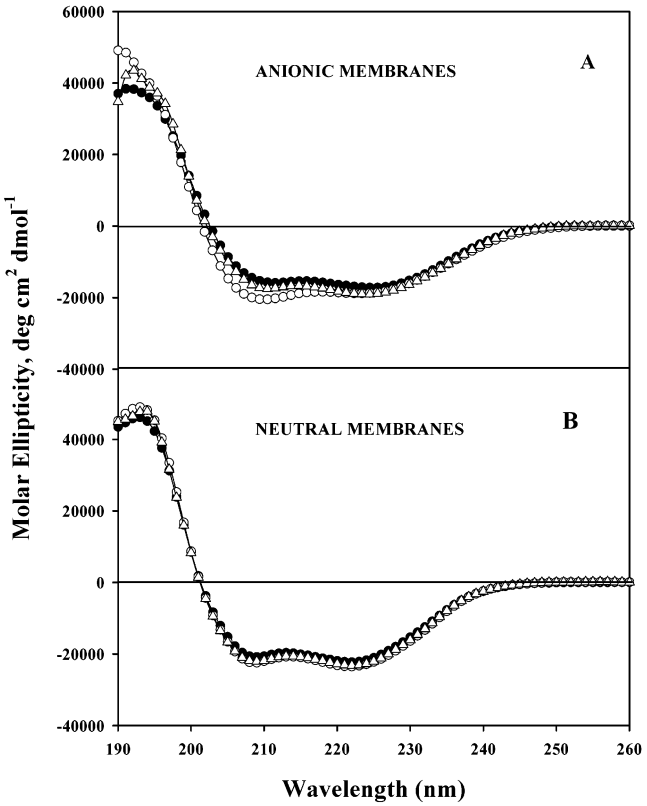


FIGURE 5: Effect of liposome surface curvature and lipid composition on mrACBP circular dichroism spectra. Circular dichroism spectra were obtained as described in Materials and Methods. In (A) symbols represent mrACBP CD spectra taken in the absence of liposome (●) and in the presence of anionic SUV (○) and anionic LUV (△). In (B) symbols represent mrACBP CD spectra taken in the absence of liposome (●) and in the presence of neutral SUV (○) and neutral LUV (△).

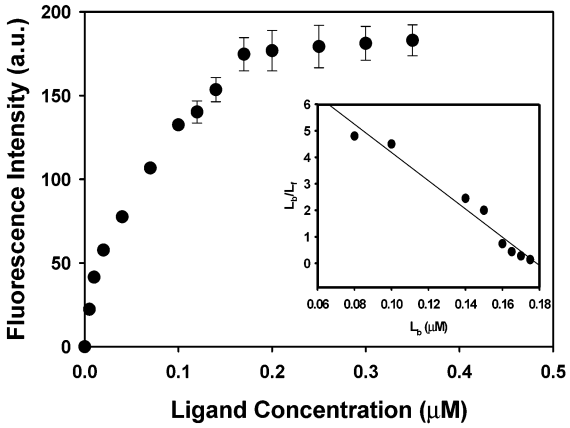


FIGURE 6: LCFA-CoA binding by mrACBP. The mrACBP (0.2 μM) was titrated with increasing *cis*-parinaroyl-CoA (0−0.4 μM). Excitation was at 310 nm, and fluorescence emission intensity reflecting binding was measured at 416 nm. All values were corrected for fluorescence emission in the absence of mrACBP. The inset represents a Scatchard plot of the *cis*-parinaroyl-CoA binding data. Values represent the mean ± SD, $n$ = 3.

*Functional Activity of mrACBP: Stimulation of Microsomal Glycerol-3-phosphate Acyltransferase (GPAT).* The functional activity of mrACBP in stimulating the rate-limiting step of microsomal phosphatidic acid biosynthesis, the first transacylation mediated by glycerol-3-phosphate acyltransferase (GPAT), was evaluated. The effect of mrACBP on microsomal phosphatidic acid synthesis was highly depend-

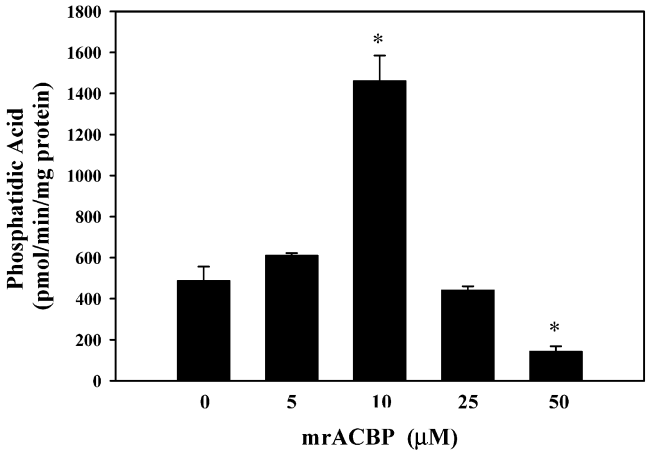


FIGURE 7: Effect of mrACBP on microsomal phosphatidic acid formation. Reactions containing 40 $\mu$M [1-$^{14}$C]oleoyl-CoA, 80 $\mu$M NaF, 15 mM DTT, 735 $\mu$M G-3-P, and 0−50 $\mu$M mrACBP in 70 mM Tris-HCl, pH 7.4, buffer were performed as described in Materials and Methods. The effect of mrACBP on microsomal phosphatidic acid formation was determined over the range 0−50 $\mu$M mrACBP. Phosphatidic acid formation was expressed as pmol min$^{-1}$ (mg of protein)$^{-1}$. Values represent the mean ± SD of triplicate determinations. Unpaired Student's *t* test was used to determine the significance of the differences. An asterisk denotes $p < 0.05$ compared to 0 $\mu$M mrACBP.

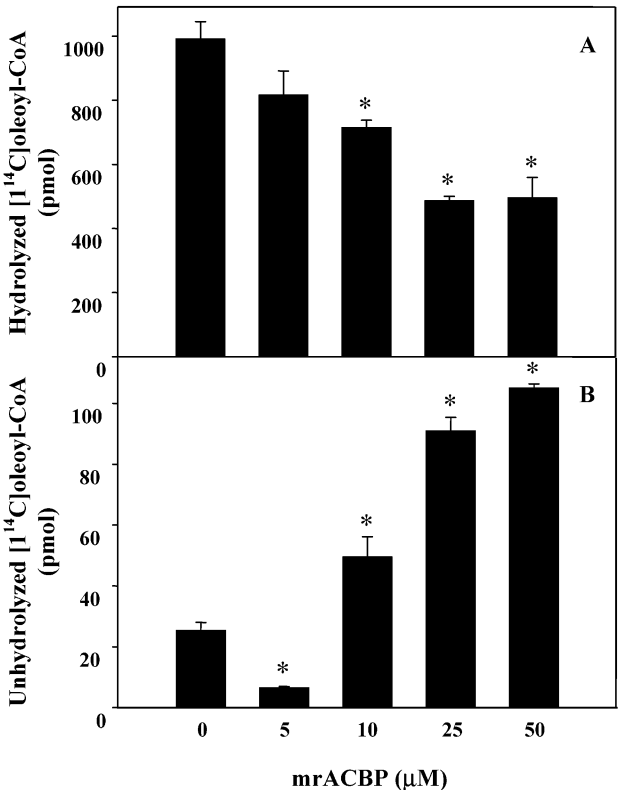


FIGURE 8: Effect of mrACBP on aqueous [1-$^{14}$C]oleoyl-CoA pool size. Panel A: hydrolyzed [1-$^{14}$C]oleoyl-CoA. Panel B: unhydrolyzed [1-$^{14}$C]oleoyl-CoA. Hydrolyzed and unhydrolyzed [1-$^{14}$C]-oleoyl-CoAs were measured in the aqueous layer and microsomes by lipid extraction and resolution of [1-$^{14}$C]oleic acid from [1-$^{14}$C]-oleoyl-CoA on gel G60 TLC plates. Reactions without mrACBP were used as control. Unpaired Student's *t* test was used to determine the significance of the differences. An asterisk denotes $p < 0.05$ compared to 0 $\mu$M mrACBP.

ent on the molar ratio of the mrACBP/oleoyl-CoA substrate. In the presence of 3-fold excess of oleoyl-CoA (40 $\mu$M), mrACBP stimulated microsomal phosphatidic acid formation 3-fold (Figure 7). This was close to the 2.3-fold stimulation previously reported in the presence of native ACBP under essentially identical conditions (*19*). In contrast, when the concentration of mrACBP (e.g., 50 $\mu$M) > oleoyl-CoA (40 $\mu$M), mrACBP inhibited microsomal phosphatidic acid synthesis by 71% (Figure 7).

*Functional Activity of mrACBP: Protection from Microsomal Fatty Acyl-CoA Hydrolase.* The ability of mrACBP to bind and thereby protect LCFA-CoA from microsomal hydrolase enzymes was determined. The data showed that mrACBP protected the oleoyl-CoA from hydrolysis in a dose-dependent manner (Figure 8A). With increasing mrACBP, microsomal hydrolysis of oleoyl-CoA decreased up to 50% (Figure 8A), similar to the effect of mouse native ACBP on microsomal hydrolysis of oleoyl-CoA (65% inhibition) (*19*).

*Functional Activity of mrACBP: LCFA-CoA Pool Size.* ACBP has been postulated to alter the partitioning of LCFA-CoA from membranes and thereby affect the aqueous pool size of LCFA-CoA (*1*). However, the results showed that this effect was highly dependent on the molar ratio of mrACBP/oleoyl-CoA. At low levels (i.e., mrACBP/oleoyl-CoA molar ratio < 1) the mrACBP reduced the amount of aqueous unhydrolyzed [1-$^{14}$C]oleoyl-CoA by 70% (Figure 8B, 5 $\mu$M mrACBP). However, this effect was not due to mrACBP enhancing [1-$^{14}$C]oleoyl-CoA hydrolysis under these conditions. Instead, the lowered level of aqueous unhydrolyzed [1-$^{14}$C]oleoyl-CoA was consistent with mrACBP stimulating [1-$^{14}$C]oleoyl-CoA utilization by acyltransferases (Figure 7) under these conditions. In contrast, under conditions of molar excess mrACBP levels (i.e., mrACBP/oleoyl-CoA molar ratio > 1) the unhydrolyzed [1-$^{14}$C]oleoyl-CoA increased up to 4.4-fold (Figure 8B). Since mrACBP inhibited [1-$^{14}$C]oleoyl-CoA utilization by acyltransferases under these conditions (Figure 7), this suggested that excess mrACBP extracted [1-$^{14}$C]oleoyl-CoA from the microsomal membrane in addition to protecting it from microsomal hydrolase activity.

*Interaction of mrACBP with Membranes: Circular Dichroism.* Although several other intracellular LCFA-CoA binding proteins such as SCP-2 (*11*, *20*) and L-FABP (*12*) interact with membranes to elicit ligand binding/transfer, it is not known if ACBP does so. Since circular dichroism (CD) measures changes in secondary structure when proteins interact with membranes (*11*, *20*, *26*), CD was utilized to determine (i) if mrACBP interacted with model membrane vesicles and (ii) the specificity of this interaction. To determine specificity, unilamellar membrane vesicles were comprised of phosphatidylcholine and cholesterol (65:35 molar ratio). To determine the effect of membrane charge, 10 mol % of palmitoyloleoylphosphatidylcholine (POPC) was replaced by 10 mol % dioleoylphosphatidylserine (DOPS), an anionic phospholipid. To determine the effect of membrane curvature, the unilamellar vesicles were prepared in two sizes, SUV and LUV, with mean vesicle diameters of 20 and 120 nm, respectively (*11*).

As indicated above, CD spectra of mrACBP in an aqueous buffer showed a negative ellipticity of −15700 deg·cm$^2$·dmol$^{-1}$ at 222 nm and a large positive ellipticity of 36430 deg·cm$^2$·dmol$^{-1}$ at 190 nm (Figure 5A, solid circles), corresponding to 56% α-helix when resolved as

Table 2: Changes in mrACBP α-Helix Content on Interaction with Liposomes

| total helix (% change) | | | |
|---|---|---|---|
| SUV | | LUV | |
| neutral | anionic | neutral | anionic |
| 3.6 ± 1.6 | 8.0 ± 3.0 | 2.6 ± 1.6 | 3.5 ± 3.8 |

described in Materials and Methods. Addition of membranes elicited small alterations in mrACBP circular dichroic spectra. In the presence of anionic SUV or LUV (Figure 5A) comprised of POPC/cholesterol/DOPS (molar ratio 55:35:10), the molar ellipticity of CD spectra at 222 nm became more negative while molar ellipticity at 190 nm became more positive. Analysis of these spectra showed that addition of anionic SUV increased the mrACBP α-helix content significantly by 8.0% (Table 2). The extent of this change was similar to that exhibited by SCP-2 upon interaction with anionic phospholipid containing SUV (*11*, *20*). However, in the presence of anionic LUV the change in the α-helix content of mrACBP was >2-fold smaller and not statistically significant. In contrast to the effects of anionic phospholipid containing SUV, the addition of neutral SUV or LUV, comprised of POPC/cholesterol (molar ratio 65:35), altered the circular dichroic spectra only slightly (Figure 5B). Analysis of the spectra showed that the increased α-helix content of mrACBP in the presence of neutral SUV and LUV was not statistically significant (Table 2).

In summary, since phospholipids and cholesterol are not ligands for ACBP (*1*), the mrACBP changes in secondary structure in the presence of anionic SUV membranes were consistent with direct interaction of the protein with the membranes. The fact that CD data showed mrACBP secondary structure changes were largest in the presence of anionic phospholipid-containing membranes that were highly curved (SUV) suggested that ionic interactions facilitated this interaction.

*Interaction of mrACBP with Membranes: Steady-State Fluorescence Spectroscopy of mrACBP Trp and Tyr.* The mrACBP contains five aromatic amino acids (Figure 4), three Tyr and two Trp, which can be excited in the 270−300 nm range and can be used to monitor changes in fluorophore microenvironment. Therefore, steady-state fluorescence spectroscopy was utilized to further analyze associations between mrACBP and anionic/neutral SUV. Upon excitation of mrACBP at 270 nm, a wavelength that excites both Tyr and Trp residues, the protein shows a broad (peak width of 69.4 ± 0.2 nm, Table 3) fluorescence emission spectrum with an emission maximum at 316.2 ± 0.9 nm (Figure 9A). Shifting the wavelength of excitation of ACBP to 296 nm, a wavelength that selectively excites Trp residues, resulted in an emission spectrum that was significantly narrowed (peak width = 65.6 ± 0.5 nm, Figure 9B) and an emission maximum that was dramatically red shifted ($\lambda_{max}$ = 332.5 ± 0.6 nm, Table 3) as compared with excitation at 270 nm.

Incubation of mrACBP with anionic SUV and excitation at 270 nm (excites both Trp and Tyr) increase emission intensity by 28% ($p < 0.001$) as compared to mrACBP alone (Figure 9A, Table 3). In addition, the emission spectrum was blue shifted by approximately 6 nm ($\lambda_{max}$ = 309.8 ± 0.5), and there was significant narrowing of the spectrum (peak width = 63.2 ± 0.5 nm). By contrast, addition of neutral SUV to mrACBP and excitation at 270 nm resulted in a slightly smaller increase in fluorescence intensity as compared to that of ACBP + anionic SUV (Figure 9A, Table 3). Interestingly, the emission spectrum of ACBP + neutral SUV was also blue shifted ($\lambda_{max}$ = 308.8 ± 0.2 nm), and

Table 3: Effect of Membrane Interaction on ACBP Fluorescence Emission Characteristics[a]

| excitation (nm) | property | ACBP | ACBP + anionic SUV | ACBP + neutral SUV |
|---|---|---|---|---|
| 270 (Tyr, Trp) | maximum intensity ($\times 10^{-3}$) | 22.3 ± 0.2 | 28.6 ± 0.1[c] | 27.1 ± 0.5[c,d] |
| | emission maximum (nm) | 316.2 ± 0.9 | 309.8 ± 0.5[c] | 308.8 ± 0.2[c] |
| | peak width (nm) | 69.4 ± 0.2 | 63.2 ± 0.5[c] | 60.6 ± 0.2[c,e] |
| 296 (Trp) | maximum intensity ($\times 10^{-3}$) | 19.0 ± 0.0 | 22.1 ± 0.2[c] | 18.1 ± 0.3[b,f] |
| | emission maximum (nm) | 332.5 ± 0.6 | 331.0 ± 0.0 | 332.3 ± 1.0 |
| | peak width (nm) | 65.6 ± 0.5 | 62.4 ± 4.4 | 67.8 ± 0.8 |

[a] Spectral properties of mrACBP (1 μM) in the presence or absence of SUV (500 μM) were obtained as in Materials and Methods. Anionic SUV = POPC/cholesterol/DOPS (55:35:10) and neutral SUV = POPC/cholesterol (65:35) were prepared as described in Materials and Methods. Measurements were made in 10 mM potassium phosphate, pH 7.4, at 25 °C. Data represent the mean ± SEM ($n$ = 4). [b] $p < 0.05$ compared to ACBP. [c] $p < 0.001$ compared to ACBP. [d] $p < 0.05$ compared to ACBP + anionic SUV. [e] $p < 0.01$ compared to ACBP + anionic SUV. [f] $p < 0.001$ compared to ACBP + anionic SUV.

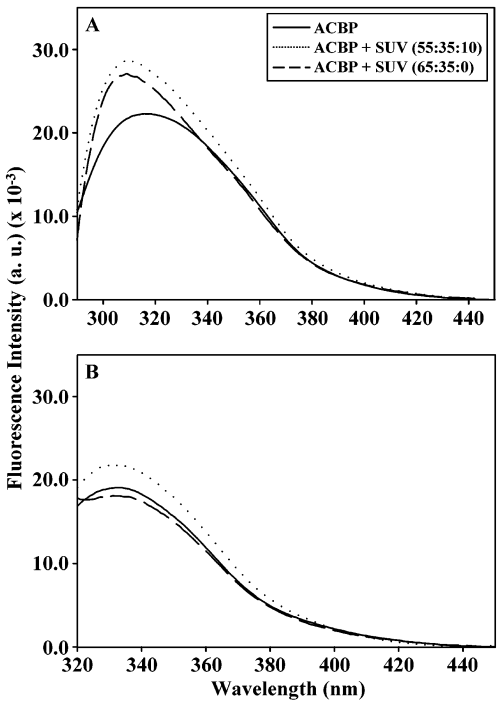


FIGURE 9: Fluorescence emission spectra of ACBP ± SUV. Fluorescence emission spectra of 1 μM ACBP were obtained with or without 500 μM SUV in 10 mM potassium phosphate, pH 7.4, at 25 °C. Anionic SUV = POPC/cholesterol/DOPS (55:35:10); neutral SUV = POPC/cholesterol (65:35). Panel A: excitation at 270 nm. Panel B: excitation at 296 nm. Each curve represents the mean of four independent scans.

the spectrum was also narrowed (peak width = 60.6 ± 0.2 nm) slightly more than that of ACBP + anionic SUV.

Excitation of ACBP + anionic SUV at 296 nm selectively excites Trp residues and increases fluorescence emission by 16% ($p < 0.001$) as compared to ACBP without SUV (Figure 9B, Table 3). By contrast, excitation of ACBP + neutral SUV at 296 nm yielded an emission spectrum that was significantly lower in fluorescence intensity than that of either ACBP or ACBP + anionic SUV. Neither anionic SUV nor neutral SUV elicited a significant change in the emission maximum or the spectrum peak width of ACBP upon excitation at 296 nm.

In summary, steady-state fluorescence analysis of the intrinsic fluorophores in mrACBP indicated that the microenvironment of Tyr, and even more so Trp, residues in mrACBP was significantly altered upon interaction with SUV membranes. The mrACBP Trp spectral changes appeared specific to anionic SUV while those from mrACBP Tyr were detected in the presence of either anionic or neutral SUV. These data provided additional evidence of an interaction between the protein and anionic membranes. Although the fluorescence data suggested some association between neutral membranes and mrACBP, these data clearly indicate that there are significant differences between anionic membranes and neutral membranes in the nature of their interactions with mrACBP. These changes in aromatic amino acid fluorescence upon mrACBP preferential interaction with anionic SUV were in the same range as those detected by circular dichroism (see above). This confirmed that interaction of mrACBP with membranes resulted in modest, but significant, alterations in mrACBP structure.

*Filtration Assay To Determine Binding of mrACBP to Membranes.* To confirm that the spectral changes exhibited by mrACBP in the presence of anionic SUV reflected direct binding to membranes, the binding experiment was repeated using a membrane filtration assay. The mrACBP was incubated with liposomes followed by separation of liposome-bound from unbound mrACBP by filtration through a 100000 Da cutoff nucleopore membrane. The filtrate containing the unbound mrACBP was then resolved by 16.5% tricine SDS−PAGE. After being stained with Coomassie Blue, the mrACBP was quantitated by Scion Image software and compared to an internal standard curve consisting of 0.1, 0.2, 0.5, and 0.8 $\mu$g of mrACBP run on the same gel.

Membrane filtration showed that 58% of mrACBP was bound to anionic phospholipid containing SUV comprised of POPC/cholesterol/DOPS at a molar ratio of 55:35:10 (Figure 10). In contrast, very little mrACBP bound to anionic phospholipid containing LUV, neutral SUV, or neutral LUV (Figure 10). This pattern of mrACBP binding specificity was similar to the pattern of circular dichroism changes (Figure 5).

These data indicated that the changes seen in the circular dichroism and fluorescence spectra and the α-helical content may be due to the binding of mrACBP to the negatively charged SUV.

*Functional Significance of mrACBP Interaction with Membranes: Transfer of mrACBP-Bound LCFA-CoA to Membranes.* As observed above, ACBP preferentially interacted with liposome membranes that contained anionic phospholipid and exhibited high surface curvature, i.e., anionic SUV. This suggested that the membrane charge and/or curvature may also affect the competence of mrACBP to donate/transfer bound LCFA-CoA to the membrane. This possibility was tested using a filtration assay to separate liposomal membrane-bound LCFA-CoA from aqueous mrACBP/LCFA-CoA. The [1-$^{14}$C]oleoyl-CoA donating assays all included samples without the liposome as controls. These controls confirmed that the filtration was efficient and reproducible.

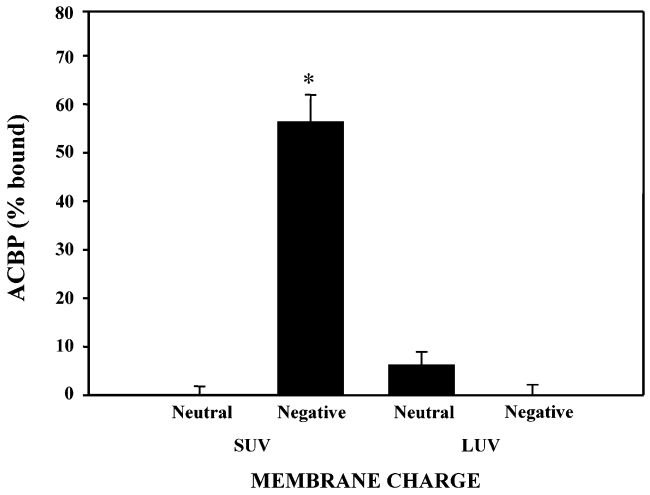


FIGURE 10: Effects of liposome surface curvature and charge on mrACBP membrane binding. The binding assay was performed as described in Materials and Methods with 2.5 $\mu$M mrACBP and 1.2 mM liposome. The percentage of unbound mrACBP was quantitated by comparison with the internal standards. The binding curve was plotted as the bound mrACBP. Each point represented the mean ± SD of triplicate determinants. The unpaired Student's *t* test was used to determine the significance of the differences. An asterisk denotes $p < 0.05$ compared to the neutral charge membrane.

In the absence of mrACBP, addition of [1-$^{14}$C]oleoyl-CoA to vesicles resulted in >98% of [1-$^{14}$C]oleoyl-CoA partitioning into membranes regardless of size and charge (Figure 11A). In contrast, addition of the mrACBP−[1-$^{14}$C]oleoyl-CoA complex to vesicles resulted in [1-$^{14}$C]oleoyl-CoA transfer to membranes with anionic SUV > anionic LUV, neutral SUV, and neutral LUV (Figure 11B). The complex of mrACBP−[1-$^{14}$C]oleoyl-CoA preferentially transferred [1-$^{14}$C]oleoyl-CoA 2.5−3-fold more to anionic SUV than to other types of membranes. These data suggested that direct binding of mrACBP to anionic SUV facilitated transfer of [1-$^{14}$C]oleoyl-CoA from the mrACBP−[1-$^{14}$C]oleoyl-CoA complex to the membrane. This transfer was optimal when the membrane was both anionic and highly curved (anionic SUV).

*Functional Significance of mrACBP Interaction with Membranes: Extraction of Membrane-Bound LCFA-CoA by mrACBP.* Since the mrACBP−LCFA-CoA complex preferentially donated LCFA-CoA to liposome membranes that contained anionic phospholipid and exhibited high surface curvature (i.e., anionic SUV), the possibility that the membrane charge and/or curvature may also affect the competence of mrACBP to extract LCFA-CoA from membranes was examined. The same filtration assay as above was used to separate membrane-bound LCFA-CoA from aqueous mrACBP−LCFA-CoA. The [1-$^{14}$C]oleoyl-CoA extraction assays all included assays without mrACBP and without liposome as controls. The controls confirmed that the filtration assay was efficient and reproducible.

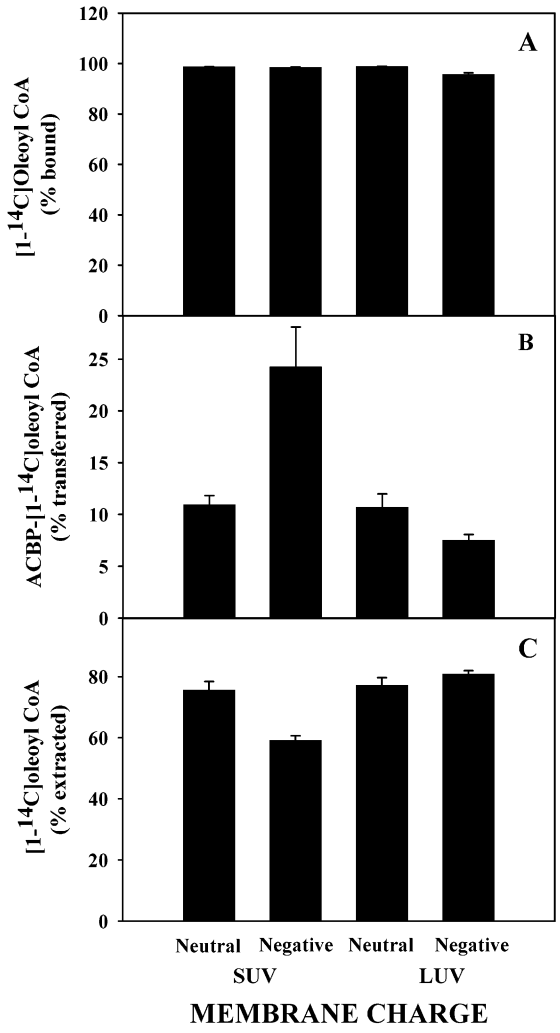


FIGURE 11: Effect of mrACBP on oleoyl-CoA partitioning. Panel A: partition of free [1-$^{14}$C]oleoyl-CoA into liposomes. Panel B: partition of mrACBP-bound [1-$^{14}$C]oleoyl-CoA to liposomes. Panel C: extraction of membrane-bound [1-$^{14}$C]oleoyl-CoA by mrACBP.

The ability of mrACBP to extract membrane-bound LCFA-CoA was dependent on both anionic phospholipid and surface curvature. The mrACBP extracted the least (about 55%) of membrane-bound [1-$^{14}$C]oleoyl-CoA from anionic phospholipid containing SUV (Figure 11C). Although all the membranes regardless of charge or curvature bound >98% of [1-$^{14}$C]oleoyl-CoA, mrACBP extracted the least [1-$^{14}$C]-oleoyl-CoA from anionic phospholipid containing, highly curved membranes. This was consistent with the most mrACBP being bound by anionic phospholipid containing, highly curved SUV membranes.

## DISCUSSION

Although most mammalian cells contain at least three families of soluble intracellular proteins that bind LCFA-CoAs, only acyl-CoA binding protein (ACBP) specifically binds only LCFA-CoAs (*1*). The structure of ACBP and its ligand binding site are now established (*5*, *6*). However, neither the physiological function(s) nor the mechanism(s) of ACBP action is (are) as yet completely resolved. In vitro studies indicate that ACBP affects the activities of both soluble and membrane-bound proteins.

ACBP affects soluble enzymes whose activities are regulated by LCFA-CoAs (*1*, *2*). For example, acetyl-CoA carboxylase is a soluble enzyme inhibited by LCFA-CoA ($K_i$ of 5.5 nM). However, under physiological levels of ACBP and LCFA-CoA, acetyl-CoA carboxylase is active. Because of the high affinity of ACBP (*1*, *2*, *6*), it has been proposed that ACBP competitively binds LCFA-CoA to maintain cellular free LCFA-CoA levels at <5 nM (*2*).

ACBP also regulates membrane-bound enzymes whose activities are either regulated by LCFA-CoA or which utilize LCFA-CoA as a substrate. For example, while neither HMG-CoA reductase nor hormone-sensitive lipase utilizes LCFA-CoA as a substrate, their activities are altered by LCFA-CoA (*1*, *2*). In contrast, a variety of membrane-bound acyltransferases directly utilize LCFA-CoA as a substrate including (i) microsomal LCFA-CoA transacylation with glycerol 3-phosphate to form phosphatidic acid (*8*, *9*, *19*), (ii) microsomal LCFA-CoA transacylation with cholesterol to form cholesteryl ester (*29*), (iii) microsomal LCFA-CoA transacylation with water (i.e., hydrolase) to form LCFA and CoA (*10*), and (iv) mitochondrial outer membrane LCFA-CoA transacylation to LCFA-carnitine (*8*, *30*−*32*). Finally, ACBP transfers LCFA-CoA between membranes (*1*, *4*, *33*). Despite these observations indicating that ACBP affects membrane protein activities, it is not known whether ACBP directly interacts with membranes. The work presented herein makes the following significant contributions to this potential interaction.

First, to examine if ACBP interacts with membranes, it was essential to utilize an ACBP that is not a variant or posttranslationally modified form. Preparations of native ACBP contain modified forms and variants of ACBP (*34*), while posttranslational modification during purification is still an issue even with recombinant ACBP. It was essential to avoid these potential problems because small differences in the ACBP amino acid sequence, especially in the N-terminus, can significantly alter its functional activity (*19*). Similar observations have been made for other LCFA-CoA binding proteins such as SCP-2 (*11*, *20*, *35*) and L-FABP (*12*). The results showed that mouse recombinant mrACBP prepared herein had amino acid sequence identical to that coded by the gene and, in addition, exhibited structure, ligand affinity, and function the same as mouse native ACBP.

Second, it was shown for the first time not only that mrACBP interacted directly with membranes but membrane binding was specific for anionic phospholipid containing membranes (i.e., anionic SUV). The interaction of mrACBP with membranes was determined by three independent methods: (i) The binding of mrACBP to membranes elicited a conformational change in mrACBP secondary structure demonstrated by circular dichroism spectroscopy. The mrACBP α-helical content increased nearly 8% in the presence of anionic phospholipid containing SUV. This effect was specific since neutral SUV did not significantly alter the mrACBP circular dichroic spectra or α-helical content. (ii) Steady-state fluorescence spectroscopy indicated significant changes in the spectral characteristics of the intrinsic mrACBP fluorophores Tyr and Trp in the presence of anionic SUV. In the presence of neutral SUV, the spectral characteristics of mrACBP Tyr and Trp were less affected. Although the changes in mrACBP emission spectra induced by association with anionic SUV were not large, they were significant ($p < 0.001$) and specific for membrane interaction as opposed to mrACBP interaction with fatty acyl-CoA

ligand, an interaction which decreased rather than increased ACBP fluorescence emission (6). Furthermore, these alterations in aromatic amino acid fluorescence upon mrACBP preferential interaction with anionic SUV were in the same range as those detected by circular dichroism, confirming that interaction of mrACBP with membranes resulted in modest, but significant, alterations in mrACBP structure. (iii) A nucleopore membrane filtration assay also showed that mrACBP bound to anionic but not neutral SUV. These data indicated that a negative surface charge was essential for facilitating interaction of mrACBP with membranes. These findings were consistent with those of other LCFA-CoA binding proteins (SCP-2, L-FABP) which also preferentially interacted with anionic SUV membranes (*11, 12, 20*).

Although the specific amino acid sequence of mrACBP responsible for membrane interactions remains to be identified, the most common secondary structure in the interfacial phospholipid binding domain of peripheral proteins and peptides is the α-helix (*36*, *37*). The three-dimensional structure of bovine apo- and holo-ACBP [determined by $^{1}H$, $^{13}C$, and $^{15}N$ NMR spectroscopy (*5*)] reveals the presence of four α-helices, A1 (Glu4−Leu15), A2 (Asp21−Val36), A3 (Gly51−Lys62), and A4 (Ser65−Tyr84) folded into an up−down−down−up helix bundle with an overhand loop between the A2 and A3 α-helices. The overall shape of the protein reveals a shallow bowl-like structure containing a hydrophobic binding region at the bottom of the bowl and a hydrophilic region at the rim of the bowl. Although all four helices are involved in ligand binding, only helices A1, A2, and A4 are important for overall protein stability (*5*). None of the A3 helix residues are involved in overall stability, and $^{15}N$ relaxation measurements upon ligand binding show a substantial decrease in $T_1$ for α-helix A1 (residues 10−16) and α-helix A3 but not the other α-helices (*5*). This indicated that α-helices A1 and A3 may be considered rather flexible structural features (*7*). Helical wheel diagrams of these α-helices demonstrated that only α-helices A3 and A4 exhibit amphipathic character with highly charged polar faces that are rich in positively charged amino acid residues (Figure 12). Such positively charged cationic faces may account for the interaction of mrACBP with phosphatidylserine (anionic, negatively charged phospholipid) in the anionic SUV membrane surface. It should be noted, however, that, in addition to these electrostatic interactions, for ACBP binding to certain membranes such as the endoplasmic reticulum an additional factor must be considered. The C-terminus of mrACBP contains the di-lysine endoplasmic reticulum retention motif (KKXX) (*38*). This di-lysine endoplasmic reticulum retention motif is highly conserved in chicken, duck, and many mammalian ACBPs and directs protein retrieval to the endoplasmic reticulum. Together, these features of ACBP provide a rational explanation that ACBP stimulates microsomal enzymes (*19*). However, in the case of other intracellular membranes, i.e., mitochondria, the endoplasmic reticulum retention motif is unlikely to play a role in ACBP action, and the electrostatic factors may be more important. Finally, it is important to note that other intracellular LCFA-CoA and LCFA binding proteins such as SCP-2 (*11, 20*), L-FABP (*12*), heart H-FABP and adipocyte A-FABP (*39*), and intestinal I-FABP (*40*) also (*41*) have amphipathic α-helix domains that interact with membranes through electrostatic interactions with anionic phospholipids.

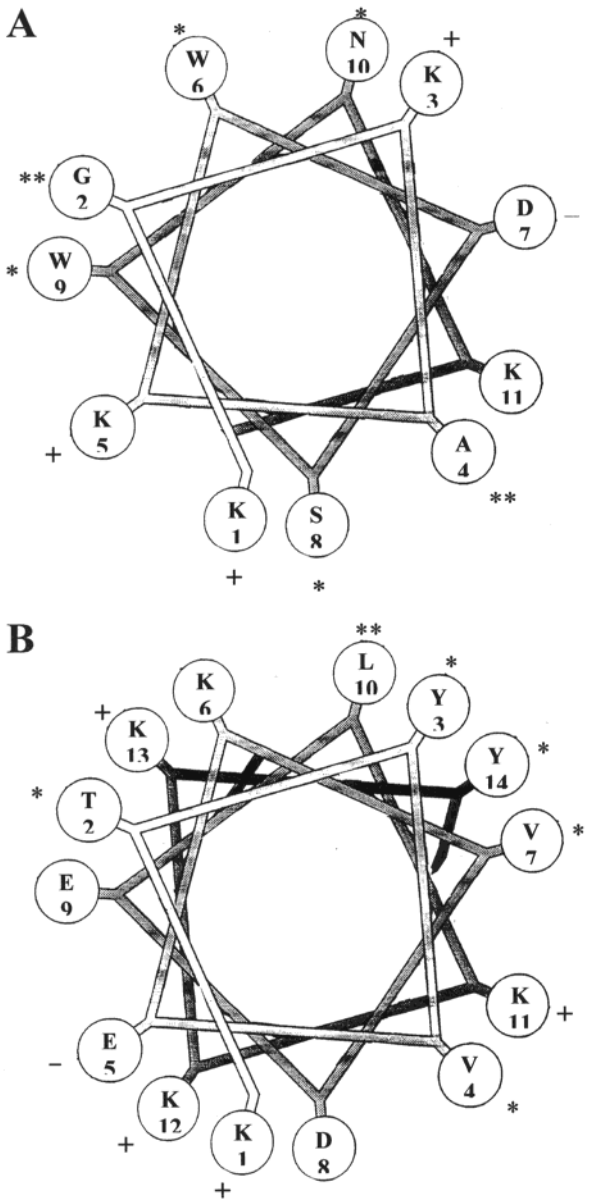


FIGURE 12: Helical wheel diagrams of mrACBP helix A3 and A4. Symbols represent (+) positively charged amino acid, (−) negatively charged amino acid, (*) polar amino acid, and (**) hydrophobic amino acid.

Third, it was shown for the first time that high surface curvature facilitated mrACBP interaction with membranes. The α-helix content of mrACBP was significantly altered in the presence of anionic SUV but not anionic LUV. Likewise, the membrane filtration assay also showed that mrACBP bound only to anionic SUV but not anionic LUV. These data indicated that not only a negative surface charge but also a high surface curvature of the membrane was important for mrACBP interaction with membranes. The mean radius of curvature of SUV is about four times smaller than that of LUV. Due to the highly curved membrane surface, it is thought that SUV are endowed with several physical properties that facilitate the binding of proteins to the SUV membrane. The packing constraints of the SUV are thought to increase exposure of the hydrophobic core of the lipid bilayer to enhance the interaction of the vesicles with hydrophobic domains of proteins (*42*). The high curvature of SUV also makes the outer monolayer more fluid

and causes more packing defects, thereby facilitating interaction with proteins (*43*, *44*). Finally, the lateral pressure of lipids in the outer monolayer of SUV is less than in LUV, further favoring protein interaction with the SUV membrane (*45*). Not only LCFA-CoA binding proteins such as mrACBP (shown herein) but other LCFA-CoA binding proteins [i.e., SCP-2 (*11*) and L-FABP (*12*)] as well as several unrelated proteins preferentially bind to highly curved SUV membranes: blood clotting Va light chain (*46*), cytochrome $b_5$ (*47*, *48*), glycosylceramidase (*42*), phospholipase A2 (*49*), and rotavirus NSP4 enterotoxin (*26*). Cell membranes are heterogeneous in membrane curvature and lipid distribution. For example, thin-section transmission electron micrographs of cultured fibroblasts reveal that the cell surface has numerous microvilli, the tips of which have diameters ranging from 13 to 50 nm (*50*). Likewise, thin-section transmission electron micrographs of the fibroblast cell surface show caveolae with "necks" (i.e., where caveolae join the plasma membrane) and "tips" having diameters of 20−30 nm (*51*−*53*). These highly curved regions of cell plasma membrane from 13 to 30 nm are in the range of the 20 ± 5 nm diameter of the SUV vesicles used herein (*11*). In contrast, the diameters of caveolae and caveolar vesicles (50−90 nm) (*51*, *52*, *54*, *55*) overlap the lower range of the 120 ± 20 nm diameter of the LUV vesicles used herein (*11*).

Fourth, taken together, the above findings suggest that the preferential interaction of ACBP with highly curved anionic membrane surfaces may be physiologically relevant. To address this question, the ability of mrACBP to donate bound LCFA-CoA to membranes and to extract membrane-bound LCFA-CoA was examined. It was shown that a mrACBP−LCFA-CoA complex preferentially donated LCFA-CoA to anionic SUV membranes. This would suggest that acyltransferases localized in anionic phospholipid-rich, highly curved membrane domains would be preferentially stimulated by mrACBP−LCFA-CoA complexes. Conversely, mrACBP was least able to extract membrane-bound LCFA-CoA from anionic SUV as compared to anionic LUV or neutral membranes. Since it is known that ACBP is an aqueous LCFA-CoA pool former and transports LCFA-CoA between membranes (*1*, *33*), this would suggest that mrACBP may preferentially extract LCFA-CoAs from neutral membrane surfaces or anionic membrane domains with low curvature in order to transfer LCFA-CoAs to anionic phospholipid-rich, highly curved membrane domains.

In conclusion, mrACBP appeared structurally and functionally the same as mouse native ACBP as evidenced by amino acid sequence, prevalence of α-helical structure, *cis*-parinaroyl-CoA binding characteristics, stimulation of microsomal phosphatidic acid synthesis, and protection from microsomal LCFA-CoA hydrolase activity. The data showed for the first time that mrACBP interacted directly with membranes, preferentially with anionic phospholipid-containing membranes that were highly curved, i.e., SUV. Thus, although it exhibits no sequence homology, mrACBP shares in common with other LCFA-CoA binding proteins (SCP-2, L-FABP) the ability to preferentially bind anionic, highly curved membranes. Interestingly, the interaction between mrACBP and anionic SUV membranes elicited a conformational change as evidenced by increased α-helix content of mrACBP. Such conformational changes in mrACBP may be important for LCFA-CoA transfer (extraction from donor membrane and donation to acceptor membrane). The mrACBP−LCFA-CoA complex preferentially donated LCFA-CoA to anionic SUV membranes and was less able to remove LCFA-CoA from anionic highly curved SUV membranes. These data suggest that both electrostatic and membrane curvature (packing) interactions may be important to the membrane binding activity and LCFA-CoA transfer functions of mrACBP. Membrane binding-induced conformational changes may alter the affinity of ACBP for oleoyl-CoA and thereby affect the ligand transfer and extraction activities.

## REFERENCES


1. Gossett, R. E., Frolov, A. A., Roths, J. B., Behnke, W. D., Kier, A. B., and Schroeder, F. (1996) *Lipids 31*, 895−918.
2. Faergeman, N. J., and Knudsen, J. (1997) *Biochem. J. 323*, 1−12.
3. Hertz, R., Magenheim, J., Berman, I., and Bar-Tana, J. (1998) *Nature 392*, 512−516.
4. Chao, H., Schroeder, F., and Kier, A. B. (2002) in *Wiley Encyclopedia of Molecular Medicine* (Creighton, T. E., Ed.) pp 44−47, J. Wiley & Sons, New York, NY.
5. Kragelund, B. B., Knudsen, J., and Poulsen, F. M. (1999) *Biochim. Biophys. Acta 1441*, 150−161.
6. Frolov, A. A., and Schroeder, F. (1998) *J. Biol. Chem. 273*, 11049−11055.
7. Rischel, C., Madsen, J. C., Andersen, K. V., and Poulsen, F. M. (1994) *Biochemistry 33*, 13997−14002.
8. Rasmussen, J. T., Faergeman, N. J., Kristiansen, K., and Knudsen, J. (1994) *Biochem. J. 299*, 165−170.
9. Jolly, C. A., Wilton, D. A., and Schroeder, F. (2000) *Biochim. Biophys. Acta 1483*, 185−197.
10. Rasmussen, J. T., Rosendal, J., and Knudsen, J. (1993) *Biochem. J. 292*, 907−913.
11. Huang, H., Ball, J. A., Billheimer, J. T., and Schroeder, F. (1999) *Biochem. J. 344*, 593−603.
12. Davies, J. K., Thumser, A. E. A., and Wilton, D. C. (1999) *Biochemistry 38*, 16932−16940.
13. Frolov, A., Cho, T. H., Billheimer, J. T., and Schroeder, F. (1996) *J. Biol. Chem. 271*, 31878−31884.
14. Stolowich, N. J., Frolov, A., Petrescu, A. D., Scott, A. I., Billheimer, J. T., and Schroeder, F. (1999) *J. Biol. Chem. 274*, 35425−35433.
15. Frolov, A., Cho, T. H., Murphy, E. J., and Schroeder, F. (1997) *Biochemistry 36*, 6545−6555.
16. Starodub, O., Jolly, C. A., Atshaves, B. P., Roths, J. B., Murphy, E. J., Kier, A. B., and Schroeder, F. (2000) *Am. J. Physiol. 279*, C1259−C1269.
17. Jolly, C. A., Chao, H., Kier, A. B., Billheimer, J. T., and Schroeder, F. (2000) *Mol. Cell. Biochem. 205*, 83−90.
18. Knudsen, J. (1990) *Mol. Cell. Biochem. 98*, 217−223.
19. Gossett, R. E., Edmondson, R. D., Jolly, C. A., Cho, T. H., Russell, D. H., Knudsen, J., Kier, A. B., and Schroeder, F. (1998) *Arch. Biochem. Biophys. 350*, 201−213.
20. Huang, H., Ball, J. A., Billheimer, J. T., and Schroeder, F. (1999) *Biochemistry 38*, 13231−13243.
21. Schagger, H., and vonJagow, G. (1987) *Anal. Biochem. 166*, 368−379.
22. Murphy, E. J., Edmondson, R. D., Russell, D. H., and Schroeder, F. (1999) *Biochim. Biophys. Acta 1436*, 413−425.
23. Rosenfeld, J., Capdevielle, J., Guillemot, J. C., and Ferrara, P. (1992) *Anal. Chem. 203*, 173−179.
24. Jolly, C. A., Murphy, E. J., and Schroeder, F. (1998) *Biochim. Biophys. Acta 1390*, 258−268.
25. Chao, H., Billheimer, J., Kier, A., and Schroeder, F. (1999) *Biochim. Biophys. Acta 1439*, 371−383.
26. Huang, H., Schroeder, F., Zeng, C., Estes, M. K., Schoer, J., and Ball, J. A. (2001) *Biochemistry 40*, 4169−4180.
27. Andersen, K. V., and Poulsen, F. M. (1992) *J. Mol. Biol. 226*, 1131−1141.
28. Owens, G. P., Sinha, A. K., Sikela, J. M., and Hahn, W. E. (1989) *Mol. Brain Res. 6*, 101−108.
29. Kerkhoff, C., Beuck, M., Threige-Rasmussen, J., Spener, F., Knudsen, J., and Schmitz, G. (1997) *Biochim. Biophys. Acta 1346*, 163−172.
30. Bhuiyan, J., Pritchard, P., Pande, S. V., and Seccombe, D. W. (1995) *Metabolism 44*, 1185−1189.

31. Bhuiyan, A. K. M. J., and Pande, S. V. (1994) *Mol. Cell. Biochem. 139*, 109−116.
32. Abo-Hashema, K. A. H., Cake, M. H., and Knudsen, J. (1999) *Biochemistry 38*, 15840−15847.
33. Knudsen, J., Jensen, M. V., Hansen, J. K., Faergeman, N. J., Neergard, T., and Gaigg, B. (1999) *Mol. Cell. Biochem. 192*, 95−103.
34. Jensen, M. S., Hojrup, P., Rasmussen, J. T., and Knudsen, J. (1992) *Biochem. J. 284*, 809−812.
35. Seedorf, U., Scheek, S., Engel, T., Steif, C., Hinz, H. J., and Assmann, G. (1994) *J. Biol. Chem. 269*, 2613−2618.
36. Epand, R. M., and Epand, R. F. (1991) in *The Structure of Biological Membranes* (Yeagle, P. L., Ed.) pp 573−601, CRC Press, London.
37. Yeagle, P. L. (1987) in *The Membranes of Cells* (Yeagle, P. L., Ed.) pp 139−168, Academic Press, New York.
38. Teasdale, R. D., and Jackson, M. R. (1996) *Annu. Rev. Cell Dev. Biol. 12*, 27−54.
39. Herr, F. M., Aronson, J., and Storch, J. (1996) *Biochemistry 35*, 1296−1303.
40. Cistola, D. P., Kim, K., Rogl, H., and Frieden, C. (1996) *Biochemistry 35*, 7559−7565.
41. Wootan, M. G., and Storch, J. (1994) *J. Biol. Chem. 269*, 10517−10523.
42. Vaccaro, A. M., Tatti, M., Ciaffoni, F., Salvioli, R., Barca, A., and Roncaioli, P. (1993) *Biochim. Biophys. Acta 1149*, 55−62.
43. Machida, K., and Ohnishi, S. I. (1980) *Biochim. Biophys. Acta 596*, 201−209.
44. Talbot, W. A., Zheng, L. X., and Lentz, B. R. (1997) *Biochemistry 36*, 5827−5836.
45. Brumm, T., Jorgensen, K., Mouritsen, O. G., and Bayerl, T. M. (1996) *Biophys. J. 70*, 1373−1379.
46. Abbott, A. J., and Nelsestuen, G. L. (1987) *Biochemistry 26*, 7994−8003.
47. Greenhut, S. F., Bourgeois, V. R., and Roseman, M. A. (1986) *J. Biol. Chem 261*, 3670−3675.
48. Taylor, K. M., and Roseman, M. A. (1995) *Biochemistry 34*, 3841−3850.
49. Wilschut, J., Regts, J., Westenberg, H., and Scherpof, G. (1978) *Biochim. Biophys. Acta 508*, 185−196.
50. Schroeder, F., Fontaine, R. N., and Kinden, D. A. (1982) *Biochim. Biophys. Acta 690*, 231−242.
51. Parton, R. G. (1996) *Curr. Opin. Cell Biol. 8*, 542−548.
52. Anderson, R. (1998) *Annu. Rev. Biochem. 67*, 199−225.
53. Schlegel, A., Volonte, D., Engelman, J. A., Galbiati, F., Mehta, P. P., Zhang, X.-L., Scherer, P. E., and Lisanti, M. P. (1998) *Cell. Signal. 10*, 457−463.
54. Brown, D. A., and London, E. (1998) *Annu. Rev. Cell Dev. Biol. 14*, 111−136.
55. Okamoto, T., Schlegel, A., Scherer, P. E., and Lisanti, M. P. (1998) *J. Biol. Chem. 273*, 5419−5422.

BI0259498